Published on 01 October 2021. Downloaded by INDIAN INSTITUTE OF TECHNOLOGY BOMBAY on 12/29/2021 7:28:32 AM.

ChemComm

COMMUNICATION

View Article Online
View Journal | View Issue

Check for updates

Cite this: *Chem. Commun.*, 2021, **57**, 11350

Received 28th June 2021,
Accepted 1st October 2021

DOI: 10.1039/d1cc03434k

rsc.li/chemcomm

In silico strategy to boost stability, axiality, and barrier heights in dysprocenium SIMs *via* SWCNT encapsulation†

Rizwan Nabi, Rupesh Kumar Tiwari and Gopalan Rajaraman *

Detailed *ab initio* CASSCF calculations coupled with periodic DFT studies on a series of $[Dy(Cp)_2]^+$ molecules encapsulated in a single-wall carbon nanotube found that encapsulation offers stability to these fragile molecules and also significantly enhances the U_{eff} values. Most importantly, this encapsulation suppresses the key vibrations responsible for reducing the blocking temperature, offering a hitherto unknown strategy for a new generation of SIM-based devices.

Single-molecule magnets (SMMs) are molecule-based magnets that exhibit permanent magnetisation similar to bulk magnets below a critical temperature called the blocking temperature (T_B).[1] This class of molecules will revolutionise current technology by offering high-density information storage devices, such as Q-bits for efficient quantum computing, and as spintronic devices driving towards robust spin transistors and spin valves.[2] Several important breakthroughs have been achieved in recent years with dysprocenium single-ion magnets (SIMs), such as $[Dy(Cp^{ttt})_2]^+$ (Cp^{ttt} = 1,2,4-tri(*tert*butyl) cyclopentadiene)[3] with a U_{eff} value of 1277 cm^{-1} and a T_B of 60 K, $[Dy(Cp^{iPr5})_2]^+$ (Cp^{iPr5} = penta-iso-propylcyclopentadienyl)[4] exhibiting a U_{eff} value of 1468 cm^{-1} and a T_B of 72 K, and $[(Cp^{iPr5})Dy(Cp^*)]^+$ (Cp^{iPr5} = penta-iso-propylcyclopentadienyl, Cp* = pentamethylcyclopentadienyl) was recently reported with a U_{eff} value of 1541 cm^{-1} and a record high T_B value of 80 K.[5] While enhancing the T_B value remains one of the goals in this area, the stability of SIMs at ambient conditions is an important gauge to realise the potential applications proposed. Secondly, retaining the magnetic properties of these SIMs on the surface is another hurdle in realising the end-user applications. Furthermore, spin reversal through phonon-assisted quantum tunnelling (QT) is the fundamental challenge in stabilising these SIMs at high temperatures.[6] It is established that the QT can be quenched using anharmonic phonons from the surface and therefore coupling the molecule to a surface offers several advantages.[7]

In this regard, here we explored the possibility of stabilising dysprocenium SIMs inside single-walled carbon nanotubes (SWCNTs) using a set of theoretical tools (*ab initio* CASSCF/RASSI-SO/SINGLE_ANISO and periodic DFT calculations). There are several experimental precedents wherein transition metals, lanthanide ions/complexes, and Ln-endohedral fullerene have been placed inside SWCNTs to obtain devices and fine-tune their properties.[8–10] The molecule, if trapped inside a SWCNT, not only exhibits stability but can also be utilised to fabricate various devices directly, as exemplified by the studies on $[TbPc_2]$@SWCNT offering spin transistors and spin valves.[11] Such devices wherein molecules are incorporated inside SWCNTs could also address the phonon-assisted QT effects as the molecules are not directly placed on the surface, offering numerous advantages in exploring this aspect.[12,13]

Here we have studied three Dy(III) complexes, $[Dy(Cp)_2]^+$, (**1**), $[Dy(Cp^{ttt})_2]^+$ (**2**), and $[(Cp^{iPr5})Dy(Cp^*)]^+$ (**3**), which were grafted in open-ended metallic armchair CNTs with smooth edges (see Fig. 1) with the reported X-ray structures of **2** and **3**[3,5] and a model (**1**) derived from these structures. Periodic DFT calculations have been performed using the PBE[14] functional incorporating dispersion effects and employing the plane-wave basis set as implemented in the CP2k program package[15,16] (see computational details for further information). Optimised geometries were then subjected to CASSCF calculations using the MOLCAS 8.0 suite[17] to obtain insight into the relaxation phenomena. The CASSCF calculations on **2** and **3** agree with earlier reports.[3,5] Further, structural optimisations were performed for **1–3** (see Fig. S1 in ESI†), and the computed geometries were consistent with the X-ray structures (see Table S2 and Fig. S1 in the ESI†). The X-ray structures of **2** and **3** yield U_{cal} values of 1354 cm^{-1} and 1424 cm^{-1}, respectively. The optimised structures also yield similar values (1273 cm^{-1} and 1409 cm^{-1} for **2opt** and **3opt**, respectively, see ESI†). To ascertain the most favourable orientation of **1** inside

Department of Chemistry, Indian Institute of Technology Bombay, Powai, Mumbai-400076, India. E-mail: rajaraman@chem.iitb.ac.in; Tel: +91-22-2576-7183

† Electronic supplementary information (ESI) available: Supporting information is available including Tables, SO states and the optimized geometries. See DOI: 10.1039/d1cc03434k

This journal is © The Royal Society of Chemistry 2021

Published on 01 October 2021. Downloaded by INDIAN INSTITUTE OF TECHNOLOGY BOMBAY on 12/29/2021 7:28:32 AM.

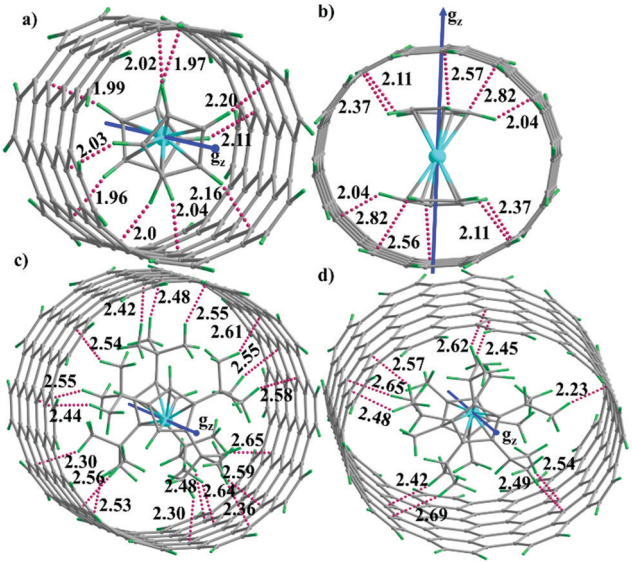

Fig. 1 DFT optimized structures: (a) **1∥@CNT**, (b) **1⊥@CNT**, (c) **2∥@CNT** and (d) **3∥@CNT**. Dotted purple lines show the closest C–H bond distances. Colour code: Dy^{III} – cyan, C – grey, and H – green. The blue arrow shows the ground state g_{zz} axis.

SWCNT(7,7), we considered two possibilities, one with the $[Dy(Cp)_2]^+$ parallel (**1∥@CNT**) to the length of the SWCNT and the other with the $[Dy(Cp)_2]^+$ perpendicular (**1⊥@CNT**) to the length of the SWCNT (see Fig. 1). The DFT computed binding energies for **1∥@CNT** and **1⊥@CNT** are −858.1 and −594.5 kJ mol^{-1}, respectively, suggesting a favourable binding (see Table S4 in ESI†). As the metal ion is not accessible for further expansion of the coordination sphere, this offers stability to these species inside the SWCNT, and this is similar to stabilising smaller fragments of Ln(III), such as Dy–O–Sc inside EMFs.[18] Further, for **1∥@CNT** additional calculations were performed to check the molecular migration inside the SWCNT, where acceptable energy penalties were found for such migration, offering confidence in device viability (see Fig. S21 in ESI†).

Moreover, we witnessed strong CH···π interactions (the shortest interaction distance at 1.96 Å) between the C–H bonds of the Cp rings and the π electrons of the SWCNT in **1∥@CNT** and moderate π···π and CH···π interactions between the Cp ring and the SWCNT in **1⊥@CNT**, offering stability to these molecules (Fig. 1). As there are several strong CH···π interactions present in **1∥@CNT**, its binding energy is larger than that of **1⊥@CNT**. In **1⊥@CNT**, there are stronger π···π interactions, which lead to the bending of C–H bonds from the plane of the ring, and this significantly weakens the CH···π interactions. Additionally, Cp–Dy–Cp was found to be slightly bent (168°) in **1∥@CNT**, while in **1⊥@CNT**, Cp–Dy–Cp was found to be linear (180°). Due to the difference in binding energy and the additional steric factors present in the Cp rings in complexes **2** and **3**, we computed only the parallel orientation for these complexes (**2∥@CNT** and **3∥@CNT**, Fig. 1(c and d)) using SWCNT(10,10), yielding binding energies of −855.2 kJ mol^{-1} and −983.6 kJ mol^{-1}, respectively (see Table S4 in ESI†). As complexes **2** and **3** have $[B(C_6F_5)_4]^-$ counter anions (CA), we performed an additional set of calculations including these anions. For these structures, the binding energies with SWCNT were found to be favourable, though the magnitudes are reduced compared to those without anions (−416 kJ mol^{-1} and −286 kJ mol^{-1} for **2-CA∥@CNT** and **3-CA∥@CNT**, respectively, see Fig. 3(a) and Fig. S15, S16 and Tables S13, S14 in ESI†).

For **1∥@CNT**, strong Ising-type g tensors ($g_x = g_y = 0.0$ and $g_z = 19.938$), with predominantly $m_J = |\pm 15/2\rangle$ being the ground state and the g_{zz} axis passing through the Cp rings, are retained inside the SWCNT (see Fig. 1(a)). The principal magnetisation axis for the first excited KD deviates from the ground-state KD by an angle of 0.4° from the g_{zz} axis of the ground state, and the largest deviation angle of 3.3° is found at the sixth excited state KD, whereas in the case of **1⊥@CNT**, the deviation is 3.8°, and the sixth doublet g_{zz} is significantly tilted compared to the ground-state KD. For **1⊥@CNT**, the computed ground-state anisotropies are $g_x = g_y = 0.000$ and $g_z = 19.907$. As we move from the ground state to the higher excited states, transverse anisotropy is prominent, resulting in the relaxation of the magnetisation *via* those states. In the case of **1∥@CNT**, the relaxation occurs *via* the 7th excited state *via* TA-QTM, thereby showing a higher U_{cal} value of 1543 cm^{-1}, while in **1⊥@CNT**, the energy barrier for magnetisation reversal is computed to be 1211 cm^{-1} and the magnetisation relaxation occurs *via* the 4th excited state (see Fig. 2, note here that the third excited state has significant tunnelling, but the larger Orbach process estimated prevents relaxation *via* this state, see ref. 19 for more details). Both the barriers are much larger than those obtained from the geometry without the SWCNT (921.3 cm^{-1}, see Table S9 in ESI†). This suggests that the SWCNT not only acts as a host and offers stability to these complexes but also enhances the Cp ligands' crystal field strength. The LoProp charge on the carbon and hydrogen atoms is enhanced significantly inside the carbon nanotube, with variations as large as −0.12 noted for **1∥@CNT** species (see Table S10 in ESI†). If we look at the difference in charge in the carbon (hydrogen) atoms of the Cp rings with and without the CNT, the enhancement in the charge is noted to be −0.362 (−0.188) for **1∥@CNT** and −0.289 (−0.14) for **1⊥@CNT** geometries (see Table S10 in ESI†). A larger effective barrier computed for **1∥@CNT** geometry is also consistent with the computed charges and the stronger CH···π interaction with CNT. Recent theoretical analysis probing the relaxation time of such a class of molecule suggests that CF is one of the key factors that control the relaxation time.[20]

Additionally, we placed the $[Dy(Cp^{ttt})_2]^+$ (**2**) and $[(Cp^{iPr5})$-$Dy(Cp^*)]^+$ (**3**) in SWCNT (see Fig. 1(c and d)) and studied their magnetic properties. *Ab initio* calculations were performed on both the geometries (**2∥@CNT** and **3∥@CNT**) after initial optimisation using DFT calculations as mentioned earlier. For geometry **2∥@CNT** (**3∥@CNT**), the computed ground-state anisotropies are $g_x = g_y = 0.000$ (0.000) and $g_z = 19.953$ (19.910) (see Table S7 in ESI†) and are strongly Ising in nature, similar to the pristine molecules, with a calculated U_{cal} value of 1163 cm^{-1} (1404.2 cm^{-1}, see Table S7 in ESI†). These values are some of the highest calculated for such a system and are

Published on 01 October 2021. Downloaded by INDIAN INSTITUTE OF TECHNOLOGY BOMBAY on 12/29/2021 7:28:32 AM.

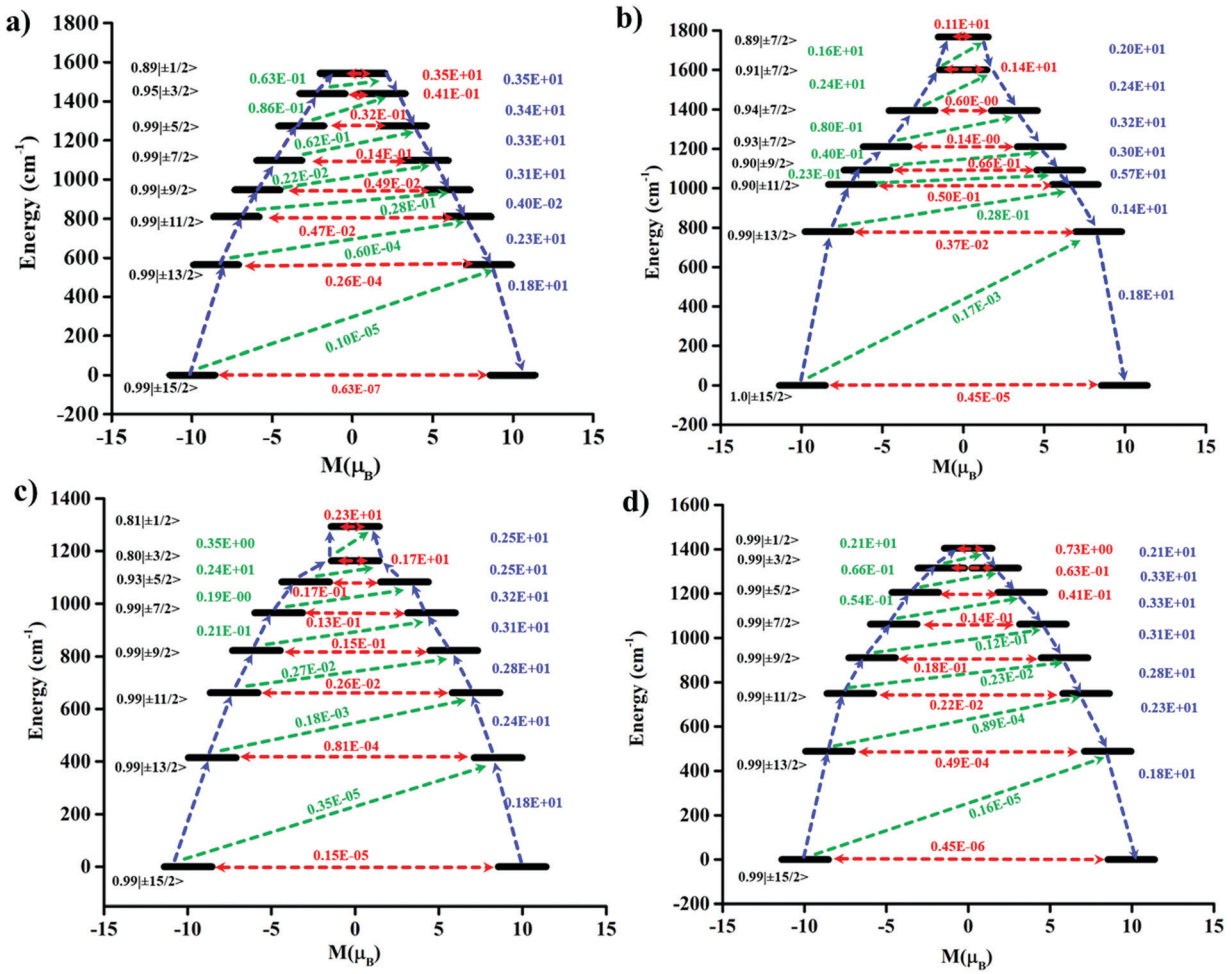

Fig. 2 *Ab initio* computed magnetisation blockade barriers, along with computed transversal magnetic moments between the connecting pairs for complexes (a) **1‖@CNT**, (b) **1⊥@CNT**, (c) **2‖@CNT**, and (d) **3‖@CNT**.

even higher than other predicted systems, such as the $[Dy(N_5)_2]^+$ and $[Dy(C_4H_4)_2]^-$ models.[21] Other computed parameters, such as ground-state m_J levels, g_{zz} axis orientation, and mechanism of magnetisation relaxation, are similar to those for **1** and **2**, except that the **2‖@CNT** is expected to relax *via* the 6th excited KD and **3‖@CNT** *via* the 7th excited KD (see Fig. 2). For the **2-CA‖@CNT** and **3-CA‖@CNT** models, the computed U_{cal} values are 1102 cm^{-1} and 1387 cm^{-1}, respectively (see Fig. S15, S16 and Tables S14, S15 in ESI†), suggesting only minor changes in the geometry/magnetic characteristics upon inclusion of counter anions.

Additionally, a Dy(III) ion is incorporated inside Stone–Wales defected SWCNT,[22] and it binds to defect site mimicking $[DyCp_2]^+$ model (see Fig. S3(e) in ESI†). For this model, *ab initio* calculations yield g_x = 0.001, g_y = 0.006, and g_z = 19.340 (see Table S8 and Fig. S6 in ESI†), with an estimated U_{cal} value of 230 cm^{-1}, with the relaxation expected to occur *via* the third excited state. This is relatively small compared to other molecules, and this is due to the weaker ligand field offered by the ring, which is part of the delocalised CNT, and a stronger transverse anisotropy offered by the carbon atoms of the other adjacent rings, similar to $[Dy(COT)_2]^-$ reports.[23,24] Secondly, it is important to note here that, apart from the U_{cal} value, T_B is key in obtaining new-generation SIMs. In the dysprocenium family of SIMs, including the ones studied here, the C–H bond vibrations of the five-membered rings have been found to be responsible for the reduction of the blocking temperature.[20] The C–H vibrations in the **1‖@CNT** are likely to be seized to a greater extent due to strong CH$\cdots\pi$ interactions and therefore could assist in obtaining larger T_B values. In the **1⊥@CNT**, although the CH$\cdots\pi$ interactions are relatively weaker, it is still likely to facilitate larger T_B values than a free dysprocenium molecule. To analyse this in detail further, we computed the frequencies on the optimised geometries using periodic DFT methods on **1‖@CNT**, which shows the largest U_{cal} value among all the models studied. Our calculations revealed that the C–H bond vibrational frequency is $\sim$200 cm^{-1} higher than the one obtained for pristine molecules as well as the X-ray structure of **2** (see Table S5 in ESI†). The C–H bond relaxes the magnetisation by causing a large distortion in the geometry, and particularly the Cp–Dy–Cp angles are substantially bent along the vibrational mode, diminishing the T_B values.[25] This bending has been proven to be an important factor in

 This journal is © The Royal Society of Chemistry 2021

Published on 01 October 2021. Downloaded by INDIAN INSTITUTE OF TECHNOLOGY BOMBAY on 12/29/2021 7:28:32 AM.

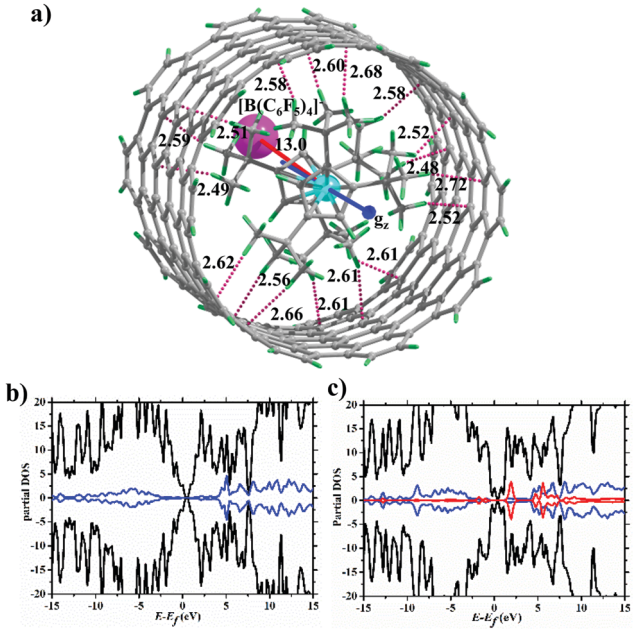

Fig. 3 (a) DFT optimized structure for **2-CA‖@CNT** (see Fig. 1 for colour code and description). For visibility, $[B(C_6F_5)_4]^-$ is shown as a pink sphere. Partial density of state (pDOS) of (b) CNT of **1‖@CNT** and (c) **1‖@CNT**. Black line corresponds to **C**, blue line corresponds to **H**, and red line corresponds to **Y**.

diminishing the blocking temperature in other Dy arene systems as well.[26] In our case, however, such bendings are prohibited due to the encapsulation in SWCNT and are therefore unlikely to cause relaxation. To check this further, we performed crystal field analysis similar to that performed for complex **2**. Several CASSCF calculations were performed along the C–H bond vibrational mode for **1‖@CNT** geometry, and the mechanism of magnetisation relaxations was then developed for these geometries, and CF parameters were analysed (see Fig. S7–S14 and Table S12 in ESI†). These calculations indicate that the molecule trapped inside the SWCNT does not relax *via* the C–H bond stretching, unlike **2**, and suggest an alternative way to increase the U_{cal} and T_B values at the same time, offering ambient-condition stability (see Fig. S7 in ESI† showing no change in the CF parameters along the vibrational mode). However, the possibility of other vibrational modes causing the relaxation cannot be ruled out.

To further understand the effect of encapsulation, the partial density of states for the pristine and encapsulated SWCNT are plotted in Fig. 3(b and c). For the pristine CNT (Fig. 3(b)), a metallic character is observed, as expected, with an extremely small gap at the Fermi level (0.0286 eV). Encapsulation reduced the metallic character in**1‖@CNT** as the gap increased to 0.3042 eV (Fig. 3(c)). Further, the hydrogen atom densities of the molecules increase while the carbon atom density of the SWCNT shows depletion of density upon encapsulation, reiterating the C–H$\cdots\pi$ interactions and p-type conductivity for the SWCNT.

To this end, we have proposed a way forward to solve multiple problems in achieving SIMs that can function at higher/room temperatures. Our work suggests that incorporating the best SIM, a dysprocenium magnet, inside a SWCNT not only significantly enhances the CF parameters and U_{cal} values, but also possesses the potential to block key vibrations responsible for a reduction in blocking temperatures.

We thank DST and SERB (CRG/2018/00430; DST/CSA-03/2018-10; SB/SJF/2019-20/12; SPR/2019/001145) for funding. RN thanks the HPC facility at the University of Manchester and ERC grant StG-851504 (PI Dr Nicholas F. Chilton) for funding.

Conflicts of interest

There are no conflicts to declare.

Notes and references

1 R. Sessoli, D. Gatteschi, A. Caneschi and M. Novak, *Nature*, 1993, **365**, 141–143.
2 L. Bogani and W. Wernsdorfer, *Nanoscience and Technology*, 2009, 194–201.
3 C. A. Goodwin, F. Ortu, D. Reta, N. F. Chilton and D. P. Mills, *Nature*, 2017, **548**, 439–442.
4 K. R. McClain, C. A. Gould, K. Chakarawet, S. J. Teat, T. J. Groshens, J. R. Long and B. G. Harvey, *Chem. Sci.*, 2018, **9**, 8492–8503.
5 F.-S. Guo, B. M. Day, Y.-C. Chen, M.-L. Tong, A. Mansikkamäki and R. A. Layfield, *Science*, 2018, **362**, 1400–1403.
6 G. Bellessa, N. Vernier, B. Barbara and D. Gatteschi, *Phys. Rev. Lett.*, 1999, **83**, 416.
7 A. Lunghi, F. Totti, R. Sessoli and S. Sanvito, *Nat. Commun.*, 2017, **8**, 1–7.
8 M. Kalbáč, L. Kavan, M. Zukalová, S. Yang, J. Čech, S. Roth and L. Dunsch, *Chem. – Eur. J.*, 2007, **13**, 8811–8817.
9 M. Del Carmen Giménez-López, F. Moro, A. La Torre, C. J. Gómez-García, P. D. Brown, J. Van Slageren and A. N. Khlobystov, *Nat. Commun.*, 2011, **2**, 1–6.
10 R. Nakanishi, J. Satoh, K. Katoh, H. Zhang, B. K. Breedlove, M. Nishijima, Y. Nakanishi, H. Omachi, H. Shinohara and M. Yamashita, *J. Am. Chem. Soc.*, 2018, **140**, 10955–10959.
11 M. Urdampilleta, N.-V. Nguyen, J.-P. Cleuziou, S. Klyatskaya, M. Ruben and W. Wernsdorfer, *Int. J. Mol. Sci.*, 2011, **12**, 6656–6667.
12 K. Irländer and J. Schnack, *Phys. Rev. B*, 2020, **102**, 054407.
13 A. Repollés, A. Cornia and F. Luis, *Phys. Rev. B: Condens. Matter Mater. Phys.*, 2014, **89**, 054429.
14 J. Paier, R. Hirschl, M. Marsman and G. Kresse, *J. Chem. Phys.*, 2005, **122**, 234102.
15 B. G. Lippert, J. Hutter and M. Parrinello, *Mol. Phys.*, 1997, **92**, 477–488.
16 J. VandeVondele, M. Krack, F. Mohamed, M. Parrinello, T. Chassaing and J. Hutter, *Comput. Phys. Commun.*, 2005, **167**, 103–128.
17 F. Aquilante, J. Autschbach, R. K. Carlson, L. F. Chibotaru, M. G. Delcey, L. De Vico, I. Fdez. Galván, N. Ferré, L. M. Frutos, L. Gagliardi, M. Garavelli, A. Giussani, C. E. Hoyer, G. Li Manni, H. Lischka, D. Ma, P. Å. Malmqvist, T. Müller, A. Nenov, M. Olivucci, T. B. Pedersen, D. Peng, F. Plasser, B. Pritchard, M. Reiher, I. Rivalta, I. Schapiro, J. Segarra-Martí, M. Stenrup, D. G. Truhlar, L. Ungur, A. Valentini, S. Vancoillie, V. Veryazov, V. P. Vysotskiy, O. Weingart, F. Zapata and R. Lindh, *J. Comput. Chem.*, 2016, **37**, 506–541.
18 A. N. Khlobystov, K. Porfyrakis, M. Kanai, D. A. Britz, A. Ardavan, H. Shinohara, T. J. S. Dennis and G. A. D. Briggs, *Angew. Chem., Int. Ed.*, 2004, **43**, 1386–1389.
19 J. Liu, C.-G. Cao, H.-B. Sun, X. Zhang and D. Niu, *J. Am. Chem. Soc.*, 2016, **138**, 13103–13106.
20 D. Reta, J. G. Kragskow and N. F. Chilton, *J. Am. Chem. Soc.*, 2021, **143**(15), 5943–5950.
21 K. Kotrle and R. Herchel, *Inorg. Chem.*, 2019, **58**, 14046–14057.
22 J.-C. Charlier, *Acc. Chem. Res.*, 2002, **35**, 1063–1069.
23 S. K. Singh, T. Gupta, L. Ungur and G. Rajaraman, *Chem. – Eur. J.*, 2015, **21**, 13812–13819.
24 L. Ungur, J. J. Le Roy, I. Korobkov, M. Murugesu and L. F. Chibotaru, *Angew. Chem., Int. Ed.*, 2014, **53**, 4413–4417.
25 L. Ruan, J. Tong, L. Li, F. Luo, R. Zhang, G. Qin and X. Zhang, *Appl. Phys. Lett.*, 2020, **117**, 072406.
26 P. Evans, D. Reta, G. F. Whitehead, N. F. Chilton and D. P. Mills, *J. Am. Chem. Soc.*, 2019, **141**, 19935–19940.